Turkish Journal of Civil Engineering, 2025, xxxx-xxxx, Paper xxx, ***Research Article***

Experimental and Numerical Investigation on Strengthening Techniques for Double-Wythe Stone Masonry Walls

Bilge DORAN[1]
Yasin Murat HOTHOT[2*]
Burcu DİNÇ ŞENGÖNÜL[3]
Metin KARSLIOĞLU[4]
Serhan ULUKAYA[5]
Nabi YÜZER[6]

ABSTRACT

Masonry structures represent the architectural and cultural heritage of great historical importance. They have been used for public and residential buildings for several thousand years. Many well-preserved old masonry structures still exist, proving that this construction can overcome loads and environmental impact. These structures have been exposed to lateral and vertical loads and atmospheric influences throughout their lives. In masonry structures, undesirable damage, cracks, and voids may occur due to environmental factors or various natural disasters, such as earthquakes, which may cause the structure to collapse. Different conventional strengthening techniques are available depending on the purpose required for stone masonry walls. This study aims to evaluate the structural behavior of double-wythe travertine stone masonry walls strengthened by carbon fiber reinforced polymer (CFRP). For this purpose, two masonry stone walls, which are made of saw-cut travertine stones and constructed with English bond, a pattern formed by laying alternate courses of stretchers and

Note:
- This paper was received on July 16, 2024 and accepted for publication by the Editorial Board on January 15, 2025.
- Discussions on this paper will be accepted by xxxxxxx xx, xxxx.

• https://doi.org/

1 Yildiz Technical University, Department of Civil Engineering, Istanbul, Türkiye
doran@yildiz.edu.tr - https://orcid.org/0000-0001-6703-7279

2 Yildiz Technical University, Department of Civil Engineering, Istanbul, Türkiye
yasinmurathothot1@gmail.com - https://orcid.org/0000-0002-7785-5141

3 Yildiz Technical University, Department of Civil Engineering, Istanbul, Türkiye
bdinc@yildiz.edu.tr - https://orcid.org/0000-0001-8450-3921

4 Yildiz Technical University, Department of Civil Engineering, Istanbul, Türkiye
metinkarslioglu91@gmail.com - https://orcid.org/0000-0002-1993-4511

5 Yildiz Technical University, Department of Civil Engineering, Istanbul, Türkiye
serhanu@yildiz.edu.tr - https://orcid.org/0000-0001-6177-1739

6 Yildiz Technical University, Department of Civil Engineering, Istanbul, Türkiye
nyuzer@yildiz.edu.tr - https://orcid.org/0000-0003-0269-0140

* Corresponding author

headers, were constructed and tested under in-plane monotonic lateral load and constant axial load. Lateral load-displacement relations and failure mechanisms were discussed. In addition, triaxial compression tests of stone, mortar, grout, and stone-mortar composite materials were performed to determine constitutive relationships. Furthermore, three-dimensional (3D) nonlinear finite element analysis (NLFEA) of stone masonry walls using the Drucker-Prager (DP) yield criterion was performed for unstrengthened stone masonry walls and strengthened ones with grout injection and CFRP. The study findings revealed that the proposed numerical modeling approach can accurately predict the experimental lateral load-displacement behavior of both strengthened and unstrengthened specimens subjected to in-plane combined axial loading and shear. Additionally, the model demonstrated its capability to simulate the experimental load-displacement and cracking patterns effectively.

Keywords: Carbon fiber reinforced polymer, double-wythe stone walls, grout injection, historical masonry structures, strengthening.

1. INTRODUCTION

Masonry buildings have been widely used for public and residential purposes for several thousand years in many countries of the world, including Türkiye. Besides, the masonry buildings represent a substantial portion of the architectural and cultural heritage that must be preserved and safely handed down to future generations. Masonry buildings have been exposed to lateral loads such as earthquakes and environmental effects throughout their service life. The main structural elements forming masonry structures are masonry walls. These walls have a heterogeneous layered structure and can be damaged due to weak connections and gaps between the materials constituting the masonry walls. Although masonry structures can bear gravitational loads, they do not exhibit adequate performance when exposed to lateral loads such as earthquakes and therefore need to be strengthened. In the literature, most of the studies have focused on specifically the strengthening techniques of masonry walls under in-plane loading [1–4]. Furthermore, many conventional techniques such as FRP, grout injection, fabric-reinforced cementitious matrix, joint repointing, fiber-reinforced paint have been currently used for strengthening masonry walls [5–8]. These techniques effectively increase strength, stiffness, and ductility of the masonry walls. However, their implementation has some drawbacks, such as being time-consuming, reducing the available space, and affecting the aesthetics of existing walls [8–10]. In recent years, the use of composite materials, such as fiber reinforced polymer (FRP) composites, to strengthen or retrofit damaged existing masonry walls has become increasingly popular, and these problems can be eliminated using these materials. FRP composites have numerous benefits, including rapid application, lightweight construction, low installation cost, resistance to corrosion, and no loss of valuable space. Carbon Fiber Reinforced Polymer (CFRP), Glass FRP (GFRP), and Aramid FRP (AFRP) are the most common types of FRP composites. FRP composites exist in different forms, i.e., rods, tendons, fabrics, and laminates, and all of these forms can be considered suitable for increasing the strength and ductility of unreinforced masonry (URM) walls [11–13].

On the other hand, grout injection is a well-established and effective technique for strengthening historical masonry walls, particularly stone masonry walls [14–16]. This method has been widely used for the repair and strengthening of existing masonry buildings

without compromising their architectural value. The main idea of the method involves injecting a grout material, which is a suspension of binder particles in an aqueous medium, into voids and fractures of the masonry wall under pressure [17–20]. The injection of grout is known to enhance the load-bearing capacity and mechanical characteristics of masonry walls by filling internal voids and cracks, thereby improving their monolithic behavior and structural integrity [17, 21].

Experimental and numerical studies have been conducted to assess the effectiveness of FRP and grout injection strengthening on masonry walls.

Bompa and Elghazouli [22] conducted experiments and numerical assessments on the shear behavior of lime mortar clay brick masonry triplets strengthened with FRP, reporting a significant strength increase ranging from 16.6% to 185.8% compared to non-strengthened counterparts.

Valluzzi et al. [23] tested three-leaf rubble stone masonry walls under compression loads. The damaged walls were strengthened with grout injection, bed joint repointing, and traverse-tying techniques. After the grout injection application, the walls were re-tested, and the maximum compressive strengths of the walls were determined. In addition, the results were validated with analytical models.

Vasconcelos et al. [24] aimed to develop reliable insight into the shear and compressive strength of stone masonry walls by conducting an experimental campaign for the characterization of stone masonry under shear and compressive loading, specifically concerning the shear behavior of dry and mortar masonry joints and the uniaxial compressive behavior of masonry prisms with distinct bed joint materials and joint surfaces. The study revealed that when designing or numerically modeling stone shear walls, it is critical to consider both the shear strength of the mortar-stone interface and the compressive strength of the masonry stone.

Mooty et al. [25] examined the effect of wall type, mortar type, and mortar thickness on the performance of limestone stone masonry walls with lime-based mortar under in-plane vertical loads up to the failure of the specimens. They determined the in-plane compressive failure load, load-deformation relationship, wall ductility, cracking pattern, and wall integrity at the failure load.

Oliveira et al. [26] conducted an experimental study on three-leaf masonry walls made of granite stone constructions from the North of Portugal. They analyzed the mechanical behavior of walls under compression and strengthened the damaged walls with GFRP and injection materials. They also investigated the walls' compressive stresses and strains and evaluated the reinforcing methods and the walls' initial state.

Rezaie et al. [27] conducted extensive cyclic shear compression tests on large rubble stone masonry walls. In this study, the impact of the axial load ratio and shear span ratio on the in-plane stiffness, strength, and drift capacity of the walls were investigated. The primary objectives of the study were to determine the cyclic behavior of rubble stone masonry walls, expand the existing database, and assess the accuracy of current models in predicting the stiffness, strength, and drift capacity of these walls based on the newly obtained data.

Estevan et al. [28] tested cylindrical stone masonry specimens using composite materials. The stone cylinder samples, used to construct the masonry specimens, were wrapped with

two types of FRP jackets and tested under uniaxial compression. The stress-axial strain curves of different samples were obtained. It was observed that the compressive strength of the stone samples reinforced with unidirectional FRP materials almost doubled.

Sandoli et al. [29] constructed squared and rectangular scaled masonry tuff columns, and some of the columns were strengthened with carbon fiber unidirectional sheets. The axial compression tests were performed on unconfined and FRP-confined prismatic tuff masonry columns. The experimental axial stress–strain curves were obtained, and the experimental results have been compared with predictive axial stress-strain theoretical models.

Rahman and Ueda [30] experimentally investigated the behavior of externally strengthened clay brick masonry walls using CFRP and polyethylene terephthalate (PET)-FRP. The results demonstrated that the in-plane shear capacity of the wall significantly increased by using both types of FRPs.

Milani et al. [31] examined the ultimate load-bearing capacity of masonry brick panels reinforced with FRP strips. They tested the panels under different loading conditions. Then, numerical models were proposed based on combined homogenization and limit analysis techniques. The experimental and numerical results regarding the lateral load-displacement relationship, failure types, and load capacities were compared.

Godio et al. [10] conducted an experimental test program and investigated the force-displacement behavior of plastered stone masonry walls made of regular sandstone blocks under shear-compression loading. The study examined the effect of the axial load ratio and load history on the walls' stiffness, strength, and drift characteristics. It validated prior findings on the impact of the axial load ratio, demonstrating that as the axial load ratio increases, the walls' initial stiffness and force capacity rise while the final drift reduces.

Ghobarah and Galal [32] investigated an effective reinforcement technique against out-of-plane overloading of masonry walls. For this purpose, five full-scale masonry walls having different opening types were constructed. The walls were laterally loaded evenly until the pre-failure state. The damaged walls were strengthened with FRP and tested again. As a result, it was stated that the lateral load-carrying capacity of the reinforced walls increased significantly and showed more ductile behavior compared to the unreinforced ones.

There are also studies by Turkish researchers on local stone walls in the literature. Bozyiğit et al. [33] reported on the findings of an investigation on 29 historic stone masonry buildings located in the cities of Hatay and Osmaniye following the 2023 Turkey earthquake sequence. Bayraktar et al. [34] examined the performance of the stone masonry buildings affected by the March 25 and 28, 2004 earthquakes in Aşkale (Erzurum). Demir and İlki [35] aimed to shed light on the mechanical characteristics of the materials and multi-leaf masonry stone walls that were widely utilized in the monumental structures of the Ottoman capital city Istanbul (Turkey). Bayraktar et al. [36] examined the dynamic response of masonry stone buildings during the July 2, 2004, Doğubayazıt (Ağrı) earthquake.

Dinç-Şengönül et al. [37] examined the performance of commercial injection material in masonry walls produced with travertine stones was determined experimentally. The aim of this article is to compare the previously applied injection application [37] by performing repair with the FRP technique on masonry walls formed with the same stone and geometry.

In line with this objective, this paper aims to evaluate the experimental and numerical lateral load-displacement relations and failure mechanisms of double-wythe stone masonry walls strengthened with double-side CFRP strips and grout injection. The experimental study was divided into two steps. In the first step, double-wythe stone masonry walls were tested under in-plane combined axial and lateral load, and the experiment was stopped once the required crack widths for grout injection application were reached on the walls. In a subsequent step, two damaged walls were strengthened using double-sided diagonal strips and grid strips CFRP with different configurations. In contrast, the others were strengthened with two different types of grouts (G1 and G2) [37]. All the strengthened walls were re-tested under the same loading protocols applied in the first step. The lateral load-displacement relations for strengthened walls were compared with unstrengthened ones. A numerical model at the macro level for 3D NLFEA was also proposed for both unstrengthened and strengthened masonry walls. Furthermore, experiments on stone, mortar, grout, and stone-mortar composite samples were carried out to evaluate the material behavior of various mortar types under triaxial compression. The characteristics obtained from the triaxial compression tests were applied to the numerical analysis of travertine stone masonry walls.

2. EXPERIMENTAL PROGRAM

2.1. Construction of Stone Walls

The experimental research was carried out in the Building Materials Laboratory of the Civil Engineering Faculty at Yildiz Technical University (YTU), Istanbul. For this purpose, Double-Wythe Stone Masonry Walls having the same geometry and material were constructed and tested under combined in-plane monotonic lateral load and constant axial load. Two stone masonry walls were planned to be strengthened with two different CFRP applications (LP_K and LP_T). To investigate the performance of masonry walls strengthened with grouting and CRFP, stone masonry walls with dimensions of 1010×1005×280 mm (length × height × width) were constructed (Fig. 1). Travertine stones, which are sedimentary rocks composed of calcium carbonate ($CaCO_3$) with dimensions of 280×135×135 mm (length × height × width), were used to construct the test walls. The mortar thickness was kept constant at 1 cm for both the bed and head joints. The mechanical properties of travertine stones are given in Table 1, respectively.

Table 1 - Mechanical properties of travertine stones [37]

	Modulus of Elasticity (GPa)	Poisson's ratio	Compressive strength of 5 cm Cube Specimen (MPa)	Flexural strength (MPa)
Travertine Stone	24 (0.5)	0.26 (0.1)	59.50 (5.0)	9.75 (1.0)

Note: Values in parentheses are standard deviation.

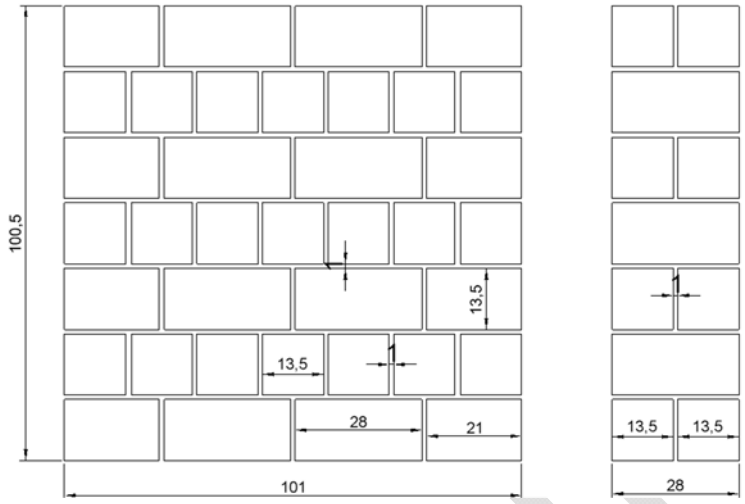

Fig. 1 - Geometry of Double-Wythe Stone Masonry Walls (All dimensions are in centimeters).

The purpose of this article is to compare the previously applied injection application by performing repair with the CFRP technique on masonry walls formed with the same stone and geometry. In accordance with this purpose, the composition recipe of mortar, the type of stones, and the geometry of stone masonry walls were used in the same way as in the previous study published by Şengönül et al. [37, 38]. Thus, two double-wythe stone masonry walls were constructed using this mixed proportion of mortar to compare two repaired stone masonry walls using grout application. The materials used in the mortar combination and their mix proportions [37] are shown in Table 2.

Generally, natural materials' physical and mechanical properties, such as travertine stone, differ significantly. Çelik and Ibrahimoglu investigated the compressive strength of travertine stones obtained from the Denizli, Emirdag-Afyonkarahisar, and Kutahya regions of Turkey. Accordingly, the compressive strength of travertine stones varies between 41 MPa and 84 MPa. Additionally, Jamshidi et al. determined the compressive strength and porosity of different travertine stones to be between 37 MPa and 66 MPa, 0.54% and 6.40%, respectively.

Dinç-Şengönül et al. [37] used two different types of grouts to determine the performance of the grout application. The first type of grout (G1) was commercial pre-mixed grout without cement, generally used to strengthen damaged existing historical buildings. This material, described as a pozzolanic lime-based injection material by the manufacturer, is frequently used to strengthen historic masonry structures. The second type of grout (G2) was produced by incorporating 30% (by weight) limestone powder into commercial grout G1. Since G2 also achieved injectability properties, it was used in the grout production, and the performance of the two grouts was compared.

Table 2 - Mix proportions of the mortar [37]

1	Mix proportions of mortar (by weight)				
	Lime putty	Sand	Limestone powder	Pozzolanic admixture	Water
Mortar	1	0.7	1	0.45	0.1

2.2. Test Setup and Instrumentation

On the 28th day after the construction, the wall was subjected to increasing lateral load under a constant, uniformly distributed vertical load. The loading apparatus consisted of 2000 kN

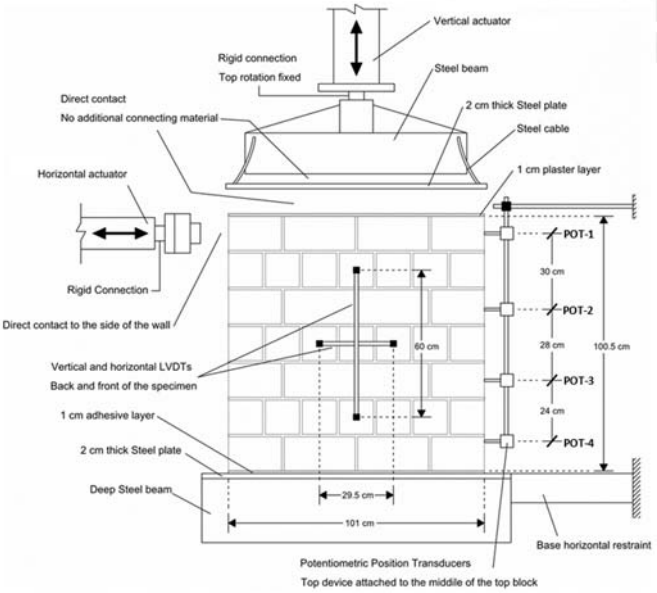

(a)

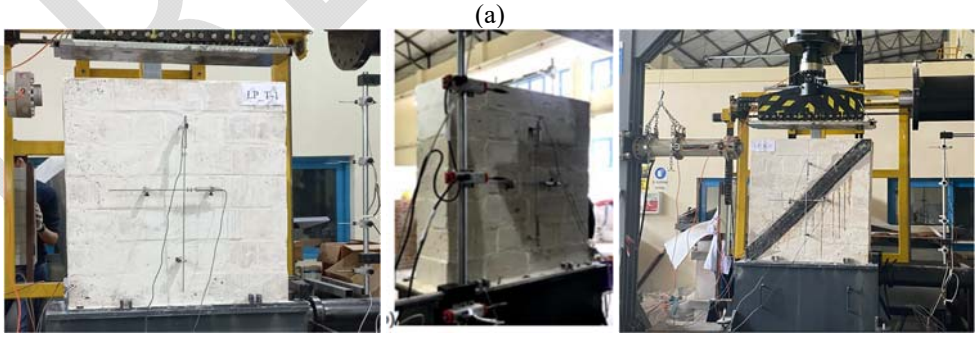

(b) (c) (d)

Fig. 2 - (a) Experimental set-up (b) LVDT set-up (front view) (c) LVDT set-up (back view) (d) Application of FRP

and 500 kN capacities hydraulic rams for vertical and lateral loading, respectively. Instrumentation included two load cells and four displacement transducers (Fig. 2). Vertical pre-compression distributed loading of 1.06 MPa (300 kN vertical load), which was kept constant during the test, was chosen based on previous experimental studies in the literature [37, 39–42]. This pre-compression load was first applied to the steel plate with a thickness of 3.5 cm located on the top of the wall. Lateral loading was then applied at a rate of 0.6±0.1 kN/s. Each wall was constructed on a rigid steel plate fixed to the steel footing in the loading frame. The measuring equipment (Fig.2) also included linear variable displacement transducers (LVDT). The modulus of elasticity of masonry (E_m) and Poisson's ratio were calculated using measurements made with LVDT. The lateral displacements at the top and bottom rows of the walls were measured by potentiometric position transducers POT1, POT2, POT3, and POT4, respectively. A data acquisition system simultaneously recorded all test data. In this study, the modulus of elasticity of stone masonry walls was determined experimentally. The modulus of elasticity for the unstrengthened wall was found to be 1900 MPa, and for the strengthened wall with grout injection, it was found to be 2250 MPa.

2.3. Strengthening of Masonry-Stone Walls

Two damaged walls were strengthened using double-sided diagonal strips and grid strips of CFRP. The others were strengthened with grout injection with different types of grouts. The performance of injection application on travertine stone walls was determined experimentally by Dinç-Şengönül et al. [37]. The primary purpose of this study is to compare the different methods by determining the CFRP performance on stone walls produced using the same materials as in previous study [37]. Therefore, two different methods were carried out independently of each other. Descriptions of the wall specimens are given in Table 3.

Table 3 - Description of wall specimens.

Unstrengthened walls		Strengthened walls	
Code	Description	Code	Description
G1	Unstrengthened Wall-1 [37]	G1-S	The wall strengthened with grout (G1) injection [37]
G2	Unstrengthened Wall-2 [37]	G2-S	The wall strengthened with grout (G2) injection [37]
LP_K	Unstrengthened Wall-3	LP_K-S	The wall strengthened with diagonal strips of CFRP on each side
LP_T	Unstrengthened Wall-4	LP_T-S	The wall strengthened with grid strips of CFRP on each side
G1, G2: Grout types; S: Strengthened; LP: Fiber polymer; K: Diagonal strips; T: Grid strips;			

Dinç-Şengönül et al. [37] produced two different injection materials to investigate the performance of injection application in masonry travertine stone walls. In this concept, only commercial injection material is used in G1 wall, while limestone powder incorporated by 30% of commercial injection material is used in G2 wall. Literature data was used to

determine the mixing procedure of injection materials. The water/binder ratio was decided according to fluidity, volume stability, and penetration limit values. According to this, as a first step in the mixing process, the powdery grout was dry-mixed to avoid agglomeration. Then, water was added within 30 seconds using the mixer, and the mixture was mixed for 8 minutes. Mechanical high-speed mixer (up to 2,000 rpm), and the stirring rate was kept constant at 2,000 rpm during the mixing process for 8½ minutes. The grouts were prepared by mixing only with water. No additive materials were used to meet satisfactory fresh grout properties because the commercial grout already contained a plasticizer.

Compressive and flexural strength of mortar and grouts were determined following EN 1015-11 [43]. Bending and subsequent compression tests were performed on the 28th, 56th, and 90th days of the hardened grout and mortar samples. The average of typical test results for the compressive and flexural strength values are given in Table 4. Elastic parameters such as the modulus of elasticity and Poisson's ratio of materials were determined according to EN 13286-43 [44]. Cylindrical samples with a diameter of 7 cm and a length of 14 cm (ϕ7/14 cm) were produced to determine the elasticity modulus and Poisson's ratio. Before the test, the trowel surfaces of the samples were capped and then subjected to a uniaxial compression test. Strain gauges were placed on the samples, and they were subjected to a compression load with a 1 mm/min loading rate in a 60-ton capacity compression machine. The load and displacements occurring during the test were recorded using a data collector, and the stress-strain curves of the samples were created using these data. A line was drawn from the starting point of the stress-strain curve to the point corresponding to 30% of the maximum stress, and the modulus of elasticity was calculated by determining the slope of this secant line [45].

Table 4 - Mechanical properties of grouts and mortar [37]

		G1	G2	Mortar
28th day	Modulus of Elasticity (MPa)	213 (20)	198 (18)	155 (15)
	Poisson's ratio	0.24 (0.01)	0.23 (0.01)	0.27(0.01)
28th day	Compressive strength (MPa)	2.0 (0.2)	1.3 (0.2)	2.5 (0.2)
	Flexural strength (MPa)	0.7 (0.1)	0.5 (0.1)	0.8 (0.1)
56th day	Compressive strength (MPa)	2.0 (0.1)	1.4 (0.1)	3.0 (0.2)
	Flexural strength (MPa)	0.7 (0.1)	0.5 (0.1)	0.8 (0.2)
90th day	Compressive strength (MPa)	2.1 (0.2)	1.6 (0.1)	3.2 (0.3)
	Flexural strength (MPa)	0.7 (0.1)	0.5 (0.1)	0.9 (0.1)

Note: Values in parentheses are standard deviation.

The uniaxial compressive strength and flexural strength under concentrated load (three-point flexural strength) of stones was performed according to suggested methods of TS EN 1926 [46], and TS EN 12372 [47] respectively. Uniaxial compressive strength tests of travertine stones were performed on 5×5×5 cm sized cubic specimens. On the other hand, to determine

the flexural strength of travertine stones 3×7×18 cm sized plate shaped samples were used. In the compressive and three-point flexural strength tests six samples were tested for each test and average values used in evaluations.

Additionally, several tests were carried out to calculate some analysis parameters (internal friction angle) for the material. Triaxial compression tests were carried out on stone, mortar, grout, and stone-mortar composite elements. The triaxial compression test machine in the YTU Building Materials Laboratory and the samples are shown in Figure 3. This test is performed to determine the shear strength parameters of cylindrical specimens subjected to triaxial compression. The approach involved gradually increasing the confining pressure to a predefined level and stabilizing it before beginning axial loading. After the specimen reached peak stress, loading was applied for a set amount of time to obtain a complete stress-strain curve. The internal friction angle was obtained as 45 degrees in the test results conducted on composite elements. Similarly, the internal friction angle was determined to be in the range of 52 to 64 degrees in the test results performed on stone samples, depending on the porosity.

Fig. 3 - Triaxial pressure system and prepared samples for experiment.

The permeability of grouts is a crucial property during their fresh state, ensuring proper flow. This property can be evaluated using the sand column test specified in the relevant standard

[48]. According to this standard, a plexiglass tube is filled with silica sand ranging from 2.0 mm to 4.0 mm, which simulates voids larger than 4 mm in diameter [16, 49–53] . Therefore, a minimum crack width of 4 mm should be achieved for injection application. In this study, observations were made throughout the wall tests, and the experiment was terminated when sufficient crack width was reached for injection application. Firstly, injection holes were drilled in a grid with lateral and vertical distances not exceeding 150–200 mm, and plastic tubes were introduced into the injection holes. Then, the cracks were cleaned with air and water injections, respectively. Finally, the grout was injected with a pressure of 1 bar starting from the bottom of the walls (Fig. 4). The injection points were sealed along the cracks with a sealing material (putty) to avoid external leakage during the injection. Relatively narrower cracks were manually filled with grout using an injection syringe. A total of 2.5 liters of injection material was used for two walls, with an average of 1.25 liters of injection material applied per wall.

Fig. 4 - The grout injection process [37].

Table 5 - Mechanical properties of CFRP.

Material	Properties			
	Modulus of elasticity E (MPa)	Tensile strength f_t (MPa)	Ultimate tensile strain (%)	Weight per unit area (g/m^2)
CFRP	≥230000	≥4900	2.1	300

The mechanical properties of CFRP composites obtained from the manufacturer are presented in Table 5. CFRP strips of 0.17 mm thickness were bonded to the walls using the procedure recommended by the manufacturer. According to this, the wall surfaces were cleaned with a wire brush. The pores in the wall specimens were sealed with a layer of primer, followed by the application of epoxy resin at the sections where CFRP was to be attached. The widths of fiber strips were constant at 50 mm for grid layout and 125 mm for diagonal layout. The sheet grid strip was then applied with resin until the resin entirely covered it. The

CFRP strips were laid on the wall in specific sections (Fig. 5). The CFRP-applied walls are shown in Fig. 5. The strengthened walls are stored in the laboratory and tested on the 28th day after the application of the CFRP.

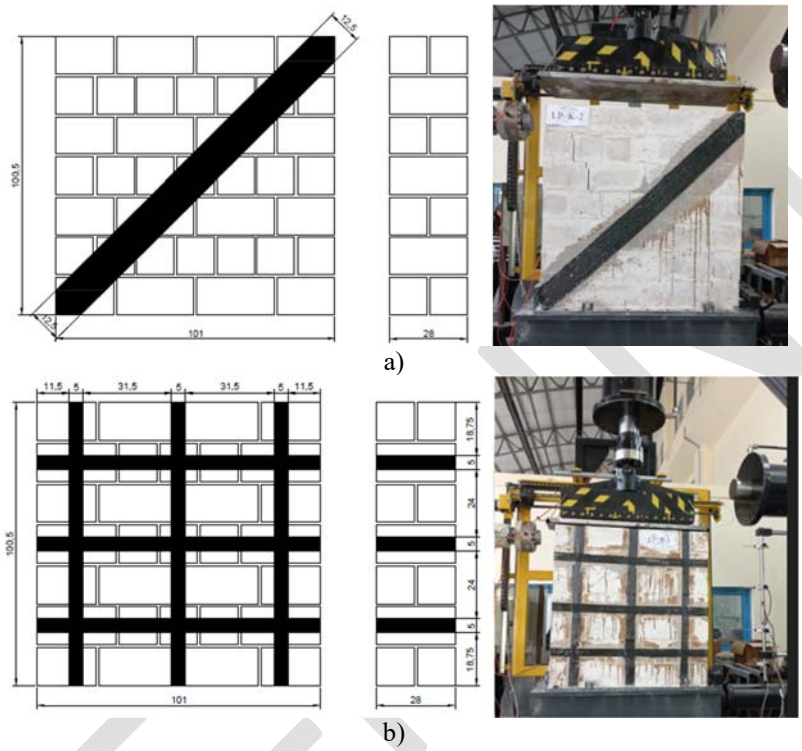

Fig. 5 - Strengthening schemes and application of CFRP (a)LP_K (b)LP_T

In the experiments performed on the unstrengthened walls, cracks propagated obviously along the diagonal direction towards the wall corners as the lateral load increased. Vertical and diagonal cracks occurred in the stone masonry units near the right toe of the wall. Observations were made throughout the wall tests, and the experiment was terminated when sufficient crack width was reached for injection application. Obtained crack patterns to the unstrengthened G1 and G2 walls are depicted in Fig. 6 and Fig. 7 respectively.

The stone walls (G1-S, G2-S), which were strengthened with the grout injection, were tested again with the same loading conditions 28 days after the injection application. Experimental cracking patterns of the G1-S and G2-S walls are given in Fig. 8 and Fig. 9, respectively. It is clearly seen that the crack widths and numbers decreased after the grout injection and the diagonal stair-step cracks were re-formed. It was observed that the crack patterns were changed, and crack width decreased from 1–8 mm to 1–4 mm after the application of the grout injections. However, it was observed that the crack pattern changed at some mortar joints, and the peak lateral load values for all walls increased.

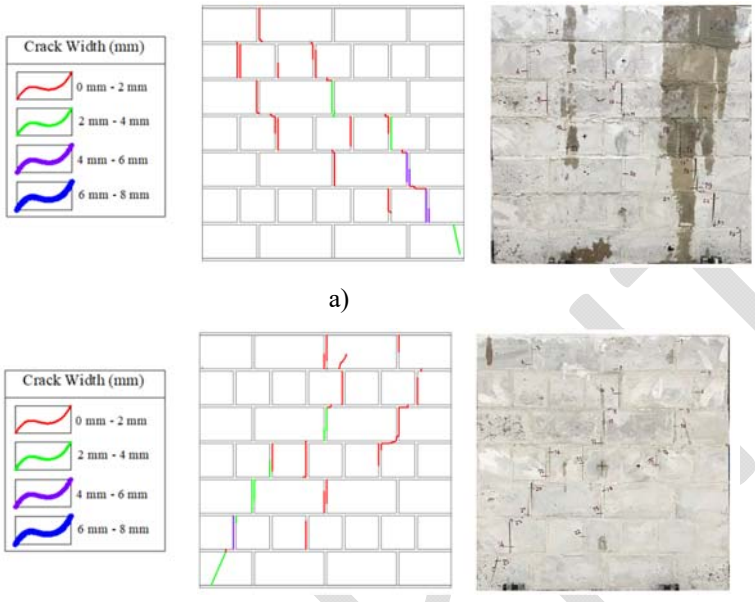

Fig. 6 - Crack patterns of G1 wall (a) front view, (b) back view [37]

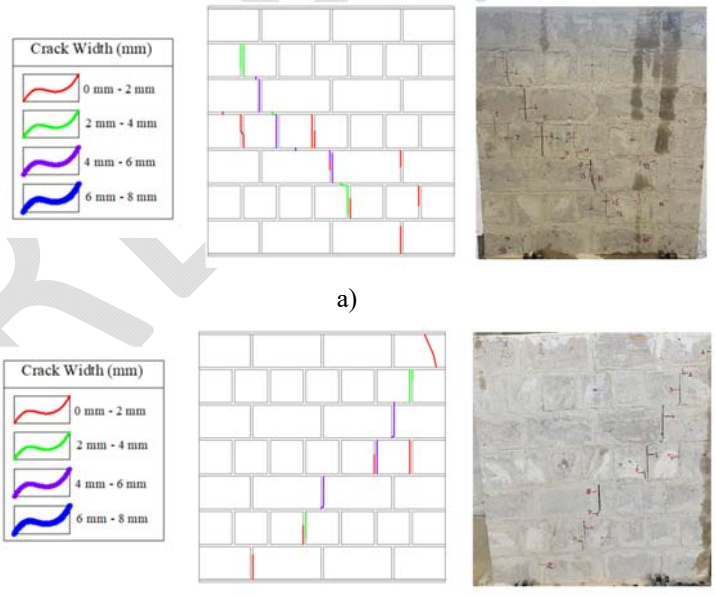

Fig. 7 - Crack patterns of G2 wall (a) front view, (b) back view [37]

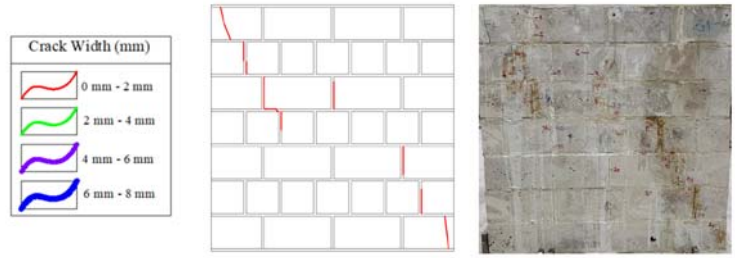

a)

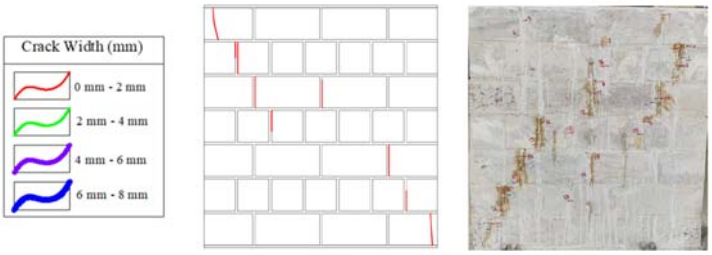

b)

Fig. 8 - Crack patterns of G1-S wall (a) front view, (b) back view [37]

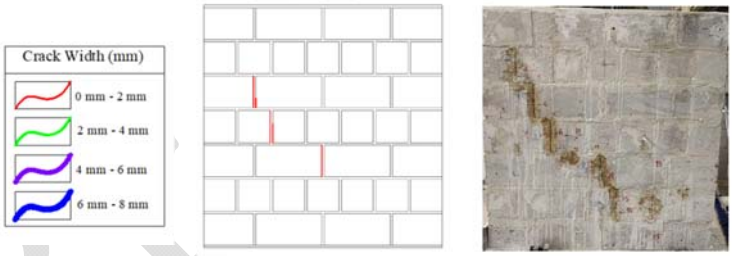

a)

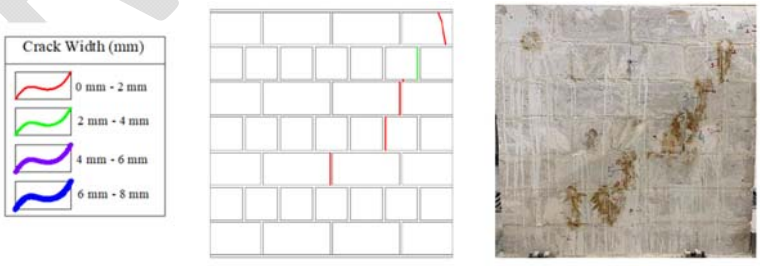

b)

Fig. 9 - Crack patterns of G2-S wall (a) front view, (b) back view [37]

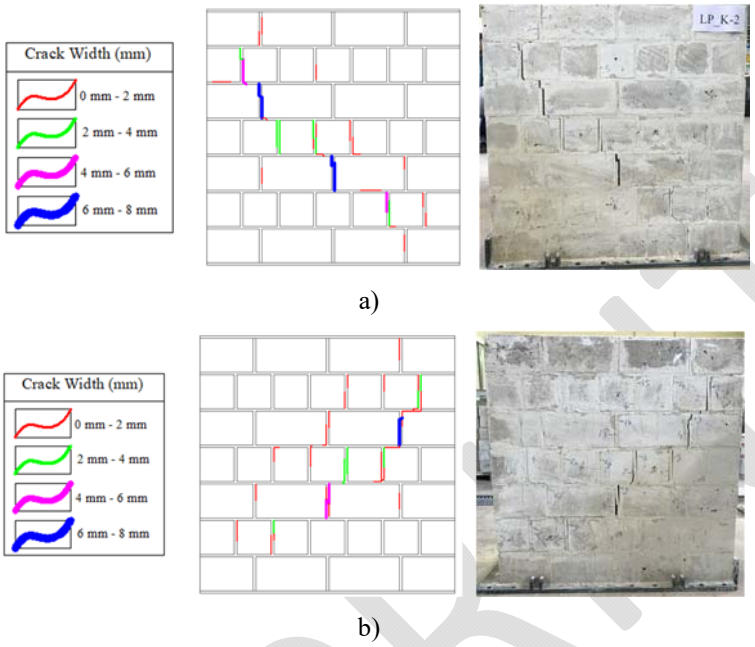

Fig. 10 - Crack patterns of LP_K wall (a) front view, (b) back view.

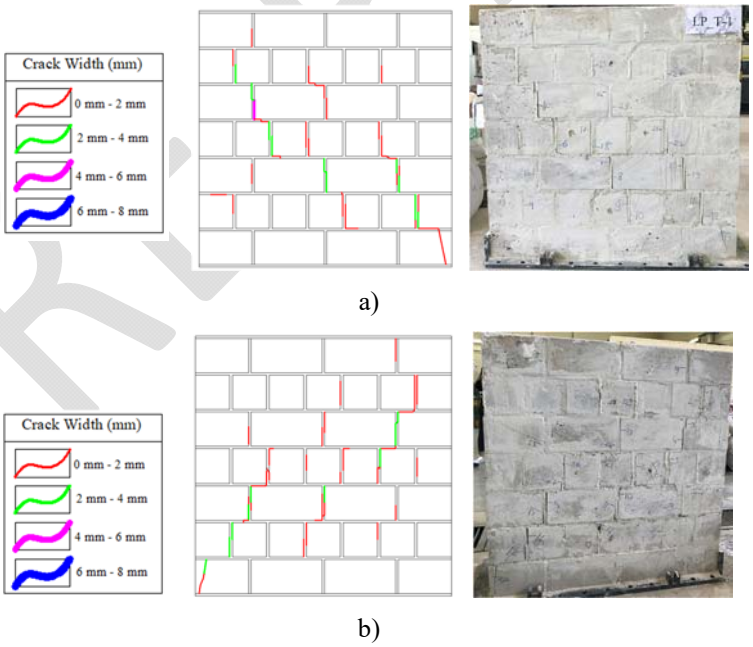

Fig. 11 - Crack patterns of LP_T wall (a) front view, (b) back view.

Similar to the procedure applied to G1 and G2 walls, LP_K and LP_T walls were also subjected to preliminary damage. Then, the damaged walls (LP_K-S, LP_T-S) strengthened with the CFRP were re-tested. Obtained crack patterns to the unstrengthened LP_K and LP_T walls are depicted in Fig. 10, and Fig. 11, respectively.

After strengthening with CFRP, observed crack patterns of the LP_K-S and LP_T-S walls are also given in Fig. 12 and Fig. 13. As can be seen in Figs. 12 and 13, the diagonal cracks were re-formed. Once the crack pattern of the walls was examined, it was noted that no new cracks occurred in these specimens. However, excessive crushing was observed in the toe regions for both specimens (Fig. 14). For all walls, the shear force capacity increased.

a) b)

Fig. 12 - Crack patterns of LP_K-S wall (a) front view, (b) back view.

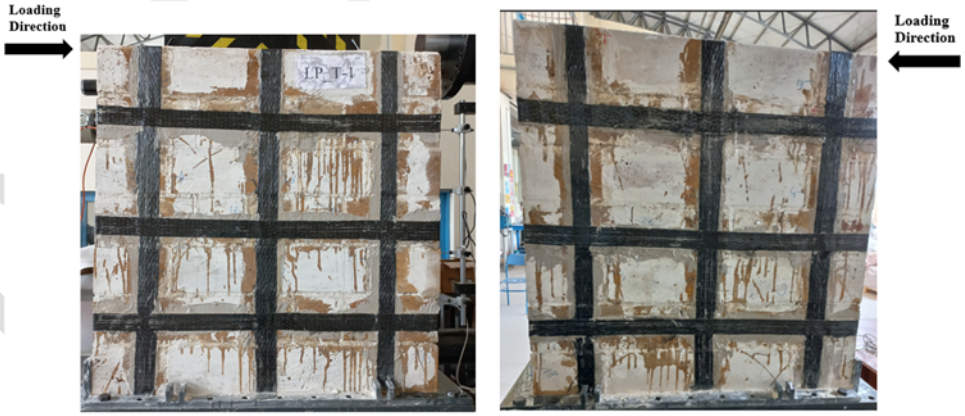

a) b)

Fig. 13 - Crack patterns of LP_T-S wall (a) front view, (b) back view.

Fig. 14 - Observed crushing failure in toe regions of the walls.

Lateral load and displacement values are summarized in Table 6. The strengthened specimens generally showed mixed failure modes, mainly characterized by shear-cracking behavior and toe-crushing for all walls.

Table 6 - Summary of test results.

Specimens	V (kN)	δ (mm)	Crack Pattern	Specimens	V_u (kN)	δ_u (mm)	Failure Mode
G1	203	12.17	DSC, TC	G1-S	250	10.19	DSC, TC
G2	208	11.52	DSC	G2-S	272	8.86	DSC
LP_K	186	12.03	DSC	LP_K-S	242	11.69	DSC, TC
LP_T	188	12.04	DSC, TC	LP_T-S	203	11.90	DSC, TC

δ: The point at which the experiment is terminated (POT-1); V: Measured lateral load corresponding to δ;
δ_u: Ultimate displacement (POT-1); V_u: Measured lateral load corresponding to δ_u; DSC: Diagonal shear crack; TC: Toe crushing;

Before strengthening, each wall was tested under the in-plane loading to stimulate pre-damage. Observations were made throughout the wall tests, and the experiment was terminated when sufficient crack width was reached. In Table 6, the experimental data obtained before and after strengthening can be assessed in terms of damage level and displacement capacity. Specifically, when evaluating the results based on damage level, the analysis can be conducted considering the drift ratio of the masonry walls. For masonry walls, seismic design codes define drift limits corresponding to different earthquake performance levels. In this context, the drift limits specified in the Turkish Seismic Code-2018 (TSC-2018), ASCE 41-13, and Eurocode-8 were reviewed. The experimentally obtained values were subsequently compared with the drift limits outlined for stone masonry walls in these codes. A summary of the drift limits provided by the design codes is presented in Table 7.

Table 7 - Performance levels and drift limits.

Performance levels	Drift ratio limits for URM Walls (%)			
	TSC-2018	Eurocode 8	ASCE 41-13	Average
Immediate Occupancy (IO) / Damage Limitation (DL)	NA	NA	0.10 (1.01)	0.10 (1.01)
Life Safety (LS) / Significant Damage (SD)	0.7 (7.04)	0.8 (8.04)	0.75 (7.54)	0.75 (7.54)
Collapse Prevention (CP) / Near Collapse (NC)	NA	1.07 (10.75)	1.00 (10.05)	1.035 (10.40)

Note: Values in parentheses are displacement value corresponding to the drift ratio limits (mm)

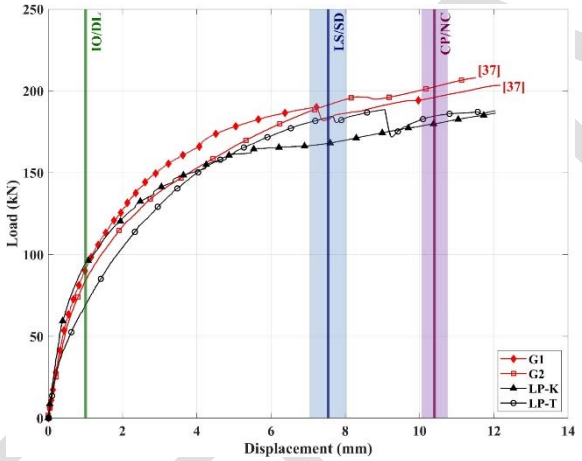

Fig. 15 - Lateral load-displacement relations and drift limits for unstrengthened wall specimens.

For the unstrengthened walls, experimental lateral load-displacement curves are presented in Fig. 15. Damage limits determined according to the codes are also marked on these curves.

When evaluating these results, it was observed that the limit values corresponding to the Immediate Occupancy (IO) performance level align with the elastic behavior region of the walls and/or the displacement level at which initial cracking occurs. The limit values for the Life Safety (LS) performance level correspond to regions where significant damage is observed, including an increase in crack widths. The Collapse Prevention (CP) performance level limit values represent regions associated with pre-failure behavior, characterized by intensified cracking and crushing in the toe regions of the walls, ultimately leading to the onset of a collapse mechanism.

The load–displacement curve for both the strengthened and unstrengthened configurations of walls G1 and G2 walls are presented in Fig.16, while those for LP_K and LP_T walls are shown in Fig.17. A comprehensive summary of the experimental results for all strengthened walls is provided in Fig.18.

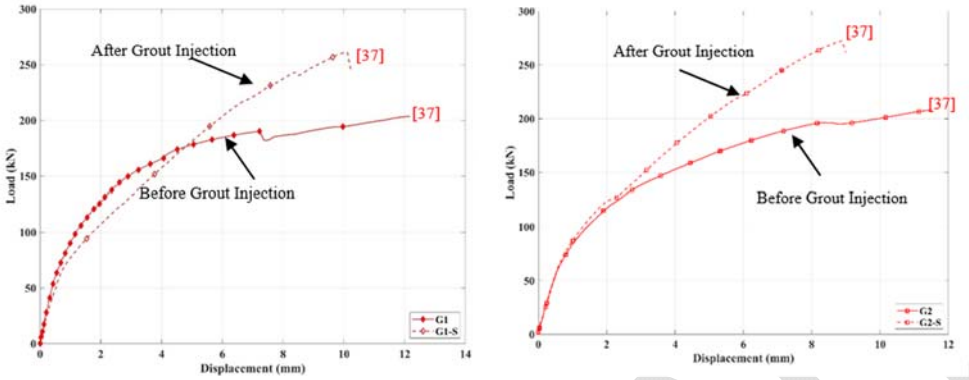

Fig. 16 - Lateral load-displacement relation before/after grout injection.

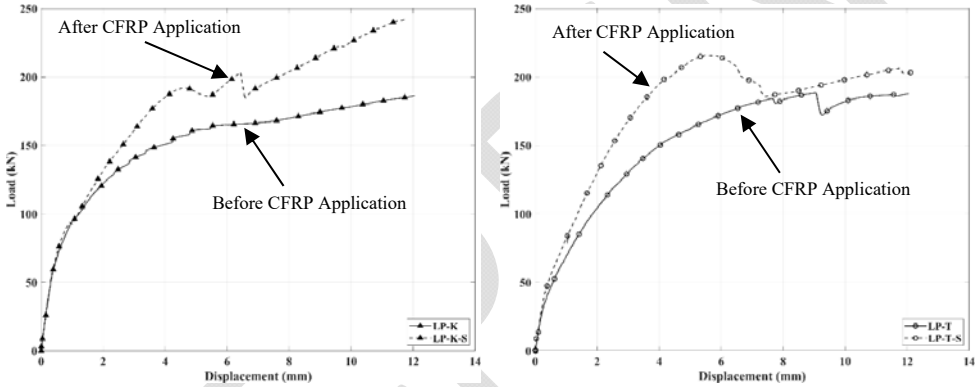

Fig. 17 - Lateral load-displacement relation before/after CFRP application.

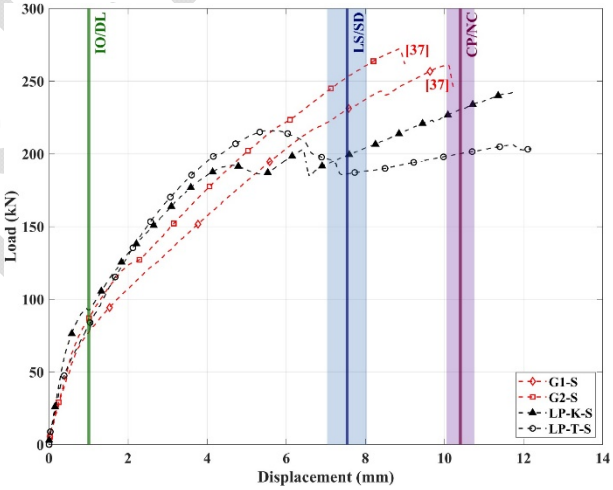

Fig. 18 - Lateral load-displacement relations and drift limits for strengthening wall specimens.

When Table 6 is examined, it is seen that the walls strengthened with CFRP have higher displacement capacity than the walls strengthened with injection. For the G1 and G2 walls, the ultimate displacement is below the limit value of collapse prevention, while the ultimate displacement is above this value in the LP_K and LP_T walls (Fig.18).

The ultimate displacement value of the LP_T-S wall is only slightly higher than that in the LP_K-S wall. However, despite the small difference in displacement, the lateral load-carrying capacity of the LP_T-S wall is 19% higher than that of the LP_K-S wall.

3. NUMERICAL ANALYSIS

Several experimental, numerical, and analytical studies have been conducted on the behavior of masonry shear walls to reach a comprehensive understanding of complex masonry behavior [2, 3, 7, 54–59] . Proposed theoretical models for implementation to NLFEA of masonry generally require many material parameters that are difficult to measure easily and reliably. For this reason, several attempts have been made to express the experimental behavior of the masonry and its constituents using different modeling techniques such as micro-modeling and macro-modeling. In micro-modeling, the masonry units, mortar, and unit-mortar interface behavior are considered. The literature has revealed that micro models are more suitable for modeling small structures, and many numerical studies showed that the interaction between mortar-stone and failure modes is essential [3, 7, 57, 60, 61] .

In the macro modeling approach, the masonry is treated as a homogeneous, isotropic continuum (Fig.19). For this reason, stone masonry units, mortar joints and interfaces are globally represented by a single element. Macro modeling is more useful for larger structures when the behavior of the entire structure is investigated.

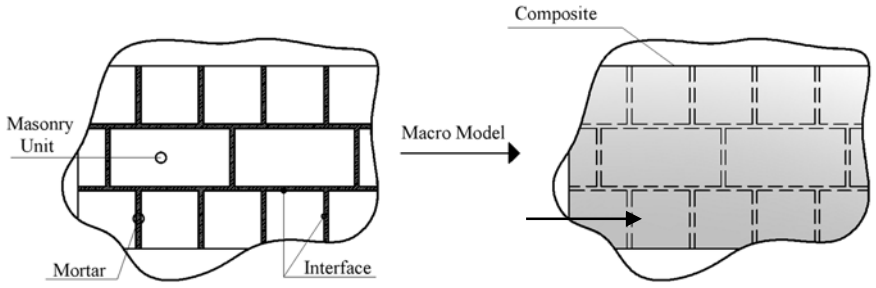

Fig. 19 - Macro modeling technique.

3.1. Constitutive Modeling

In this study, 3D NLFEA of test walls were performed by using ABAQUS-2021 software [62] with the macro-modelling approach to obtain the experimental mechanical behavior and lateral load-displacement relations (Fig.20). SI units (kN, m) were used in modeling and analysis procedures. The nonlinear constitutive behavior of masonry stone walls was represented using Drucker-Prager (DP) constitutive models. Multi-axial stress states define

the constitutive behavior of the structures, such as masonry walls, reinforced concrete panels, confined columns, or elements beyond the elastic range. The basic elastoplastic constitutive models, such as Mohr-Coulomb (MC) and Drucker-Prager (DP), have been widely adopted in the modeling of materials such as concrete, soil and rock [58, 61, 63–66].

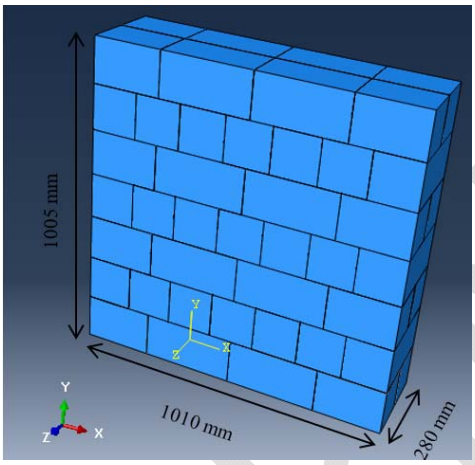

Fig. 20 - Typical geometry for unstrengthened Double-Wythe Stone Masonry Walls.

DP yield criterion is the most practical mathematical form of the von Mises criterion used for concrete, metal, and stone-type materials and takes into account both hydrostatic pressure and deviator stress effects at the highest strength (Fig. 21). Because of the smooth surface representation of the yield criterion, DP criterion (Fig.21) would be the first choice for the elastoplastic analyses:

$$f(\xi,\rho)=\sqrt{6}\,\alpha\,\xi+\rho-\sqrt{2}k=0 \tag{1}$$

where α and k are material constants; $\xi=I_1/3$ and $\rho=\sqrt{2J_2}$. I_1 and J_2 are the first invariant of the stress tensor and the second invariant of the stress deviator tensor [67] . The invariants ξ and I_1 indicate the hydrostatic component of the current stress state. Because of the incompressibility of plastic deformations only ρ can contribute to the yielding for isotropic materials. In other words, ρ is the part of the stress that tends to change shape [58].

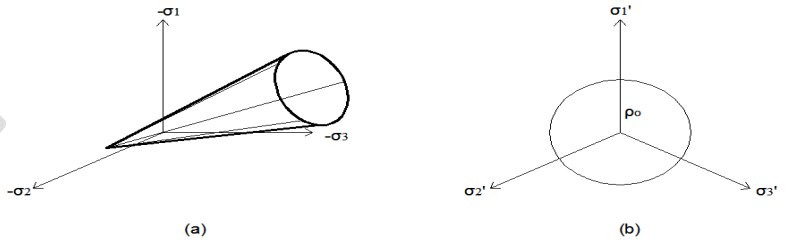

Fig. 21 - DP yield criterion (a) yield surface in the principal stress space, (b) π plane [67].

The surfaces of both DP and MC yield criteria are made to coincide along the compression meridian, as shown in Fig.22, and then the constants α and k are related to the constants c and ϕ [67]:

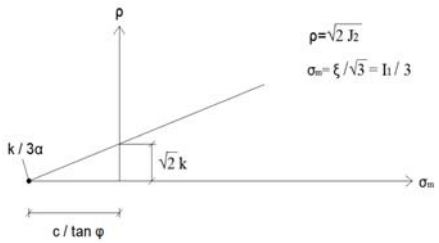

Fig. 22 - Compression meridian of DP yield criterion [67].

$$\alpha = \frac{2\sin\phi}{\sqrt{3}(3-\sin\phi)}, \quad k = \frac{6c\cos\phi}{\sqrt{3}(3-\sin\phi)} \tag{2}$$

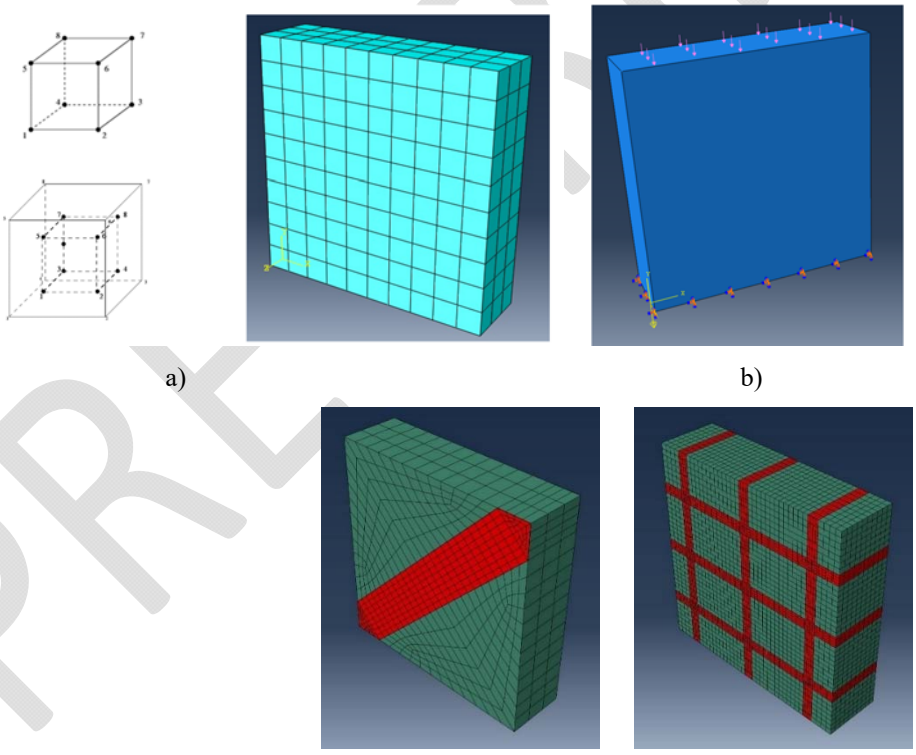

Fig. 23 - FE model a) FE mesh and brick element (C3D8) b) Boundary-loading conditions c)LP_K-S FE Model d)LP_T-S FE Model.

In this study, 3D NLFEA has been used for stone masonry walls. Masonry constituents, e.g., stone and mortar, are assumed to be isotropic, and the model is considered with an eight-node brick element (C3D8) with a DP constitutive model [61, 65, 66] in ABAQUS software [62]. Also, a lamina material model was used for CFRP elements. The mechanical parameters of the CFRP used in the analyzes are given in Table 8. Interaction behavior between the masonry wall and CFRP strips was assumed as hard contact [62] . The finite element (FE) type, mesh, and boundary-loading conditions are shown in Fig. 23.

The evolution of the yield surface with plastic deformation is described in terms of the equivalent stress $\bar{\sigma}$, which can be chosen as either the uniaxial compression yield stress, the uniaxial tension yield stress, or the shear (cohesion) yield stress [62]. In this study, hardening behavior type was selected as compression strength (σ_c).

In macro modeling, it is crucial to accurately characterize the material properties for masonry. In this paper, the most critical parameters for masonry, namely modulus of elasticity (E_m), internal friction angle (ϕ), Poisson's ratio were determined experimentally as stated in Section 2.2. Since the test walls were being strengthened after the initial loading phase, the experiments conducted under in-plane loads were terminated much before the masonry walls reached the collapse mechanism or immediately after initial cracking. Additionally, the compressive strength of the masonry walls could not be obtained experimentally so the compressive strength parameter required for numerical analysis was determined using empirical relations accepted in the literature [68–71].

The failure mechanism and lateral load-displacement behavior of masonry are strongly affected by the difference in modulus of elasticity between unit and mortar [72, 73]. In this study, the modulus of elasticity of stone masonry walls was determined experimentally (Fig. 2a). In numerical modeling, the following equation (Eq. 3) was used to determine the compressive strength of masonry wall (σ_c) [68–71].

$$E_m \approx (550 - 750)\ \sigma_c \tag{3}$$

The other material parameter used in the constitutive model is the flow stress ratio of the flow stress in triaxial tension to the flow stress in triaxial compression, *K*. 0.778≤K≤1.00. In this study, the mechanical parameters of the stone masonry walls are given in Table 8.

Table 8 - Material parameters employed in Finite Element analyses.

Stone Masonry Wall			CFRP	
DP Model	Before Strengthening	After Grout Injection		
E_m (MPa)	1900	2250	E (MPa)	230000
ϕ (^{o})	45	45	f_t (MPa)	4900
Poisson Ratio	0.28	0.28	Ultimate tensile strain (%)	2.1
σ_c (MPa)	3.25	4.00	Weight per unit area (g/m^2)	300
K	0.85	0.85		

3.2. Comparison of the Numerical and Experimental Results

The lateral load-displacement curve obtained from nonlinear FEA is compared with the experimental results before strengthening (Fig. 24a) and after grout injection (Fig. 24b).

It can be seen that the numerical results are compatible with the lateral load - displacement curve obtained from the tests before strengthening. The slopes of the initial ascending part of the load-displacement curves and the peak load-displacement levels of the unstrengthened walls agree well with the numerical results. Furthermore, the ultimate displacement and lateral load values are in close agreement with the test results (Fig. 24a).

A comparison of the numerical and experimental load-displacement responses of G1-S and G2-S specimens is given in Figure 24b. It can be said that the numerical results for the G1-S and G2-S specimens show good agreement with the experimental results in terms of the initial stiffness, ultimate displacement, and peak lateral load. Unfortunately, for both specimens, there exist major discrepancies between the predicted and experimental results for the post-elastic part of the curve. Here, it can be stated that there exists no gradually developing damage defined in the macro modeling technique with DP model.

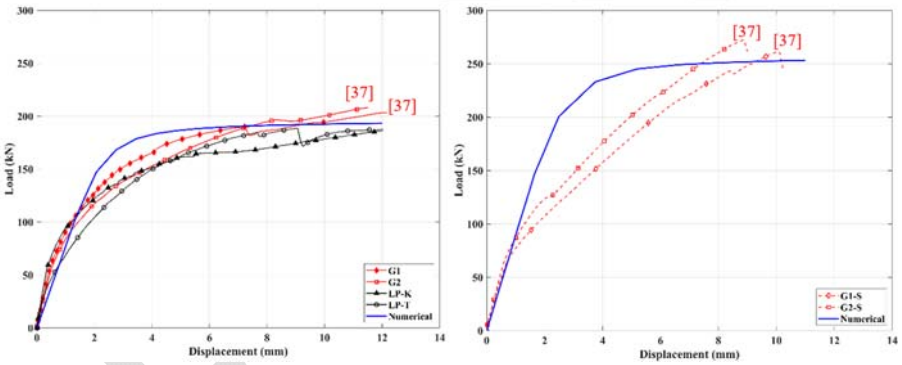

a) Before Strengthening b) After Grout Injection

Fig. 24 - Comparison of experimental and numerical analysis result for Double-Wythe Stone Masonry Walls.

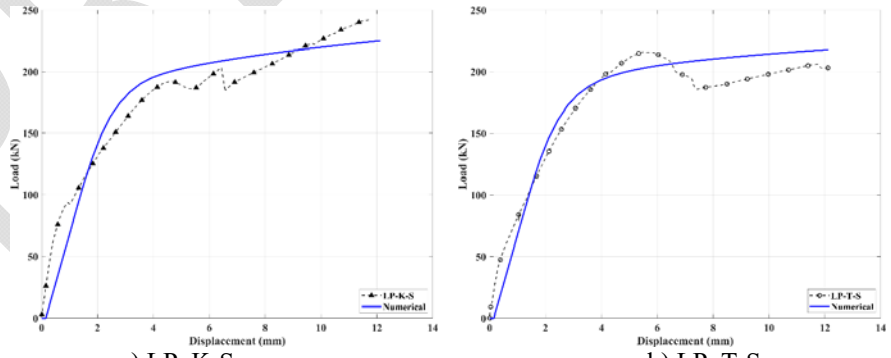

a) LP_K-S b) LP_T-S

Fig. 25 - The lateral load - lateral displacement curves for LP_K-S and LP_T-S.

The lateral load - displacement curve obtained from numerical analysis is compared with the experimental results in Fig.25a for LP_K-S and Fig.25b for LP_T-S. The numerical results are compatible with the lateral load-displacement curve obtained from the test. The post-peak behavior of the test wall is close to numerical results.

During the experiments, cracks predominantly occurred along the mortar joints in a stair-step pattern, and significant crushing was observed in the toe region of the wall (Fig. 26a). The shear stress distribution of the stone masonry wall is shown in Fig. 26b. When the test and numerical results are compared in terms of shear stress, it is evident that shear stress concentrations in the numerical results correspond to areas where crack widths have higher values.

Comparison of the numerical and experimental crack patterns was evaluated through the distribution of the maximum principal plastic strains and minimum principal stresses in Fig.26 c, d. It is observed that stress and strain values are concentrated in the toe regions of the wall.

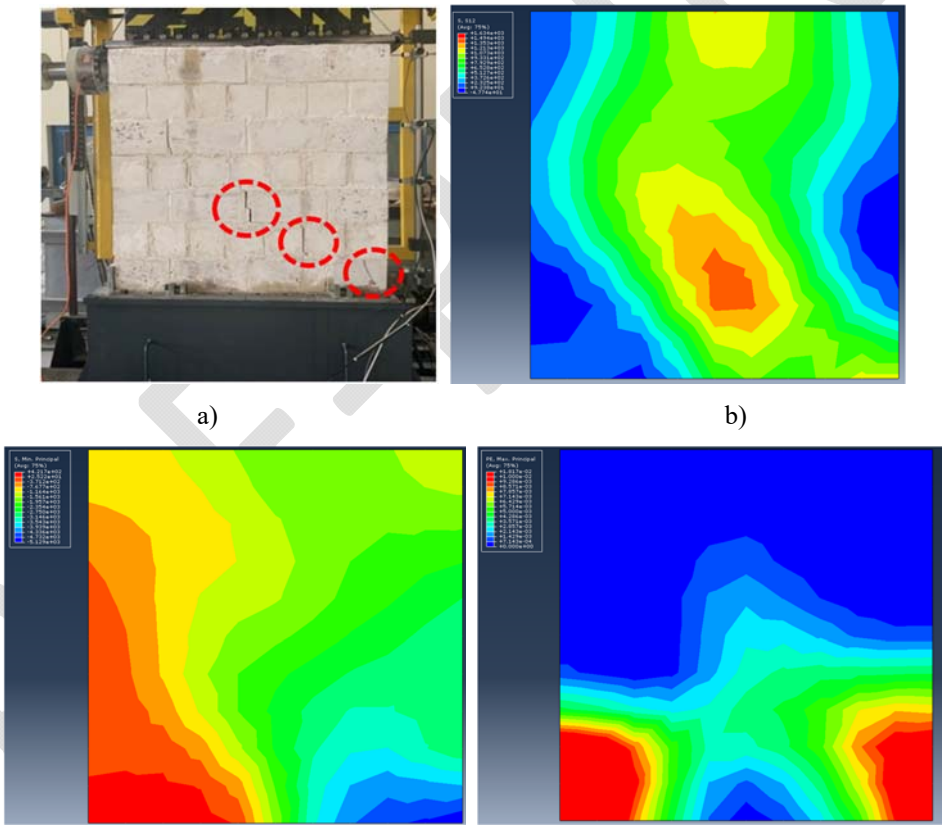

Fig. 26 - Experimental and numerical analysis result for unstrengthened walls a) Experimental crack pattern, b) Shear stress distribution, c) Minimum principal stress, d) Maximum principal strain

For LP_K-S specimen, a comparison of the experimental crack figure (Fig.27a) and shear stress distribution (Fig.27b) obtained from the numerical results is presented in Fig.27 and also, the tensile stress in the CFRP elements is given in Fig. 28. It was observed that CFRP application changed the shear stress distribution on the wall. As a result of the numerical analysis, it showed that the tensile stress in the CFRP reached to 1611 MPa. The tensile strength of CFRP is 4900 MPa and the ultimate tensile strain is 2.1%. It should also be mentioned that there was no debonding of CFRP from the surface of the wall during the test. It can be said that numerical results are compatible with experimental ones.

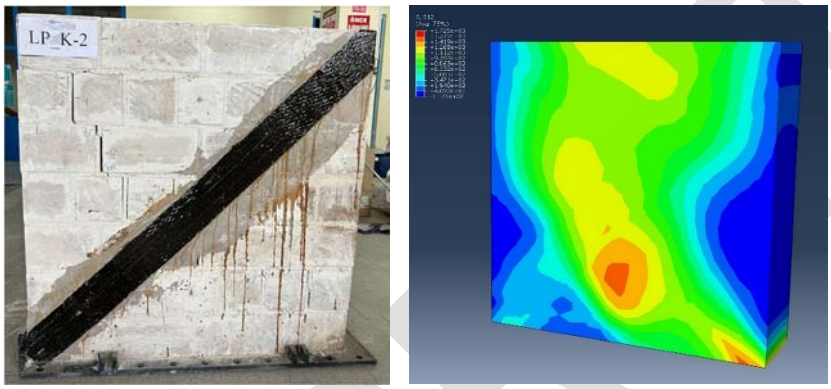

a) b)

Fig. 27 - Experimental and numerical analysis results for LP_K-S. a) Experimental crack pattern, b) Shear stress distribution

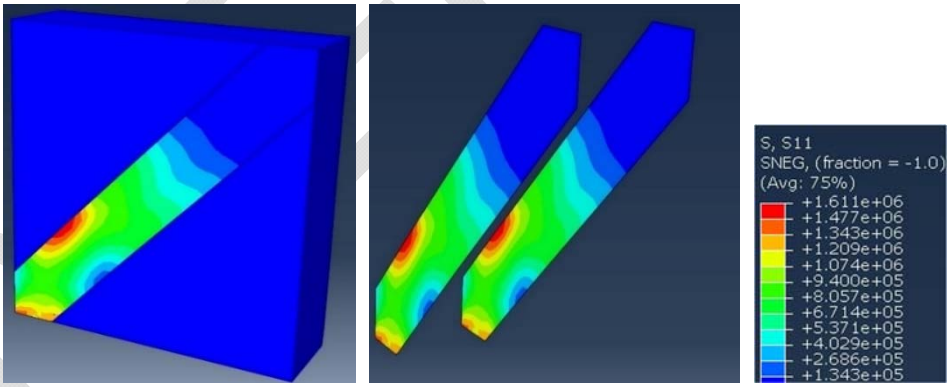

Fig. 28 - Tensile stress distribution in CFRP of LP_K-S.

For LP_T-S specimen, a comparison of the experimental crack figure (Fig.29a) and shear stress distribution (Fig.29b) obtained from the numerical results is presented in Fig. 29 and also, the tensile stress in the CFRP elements is given in Fig. 30. It was observed that CFRP application changed the shear stress distribution on the wall. As a result of the numerical

analysis, it showed that the tensile stress in the CFRP reached to 2794 MPa. The tensile strength of CFRP is 4900 MPa and the ultimate tensile strain is 2.1%. It should also be mentioned that there was no debonding of CFRP from the surface of the wall during the test. It can be said that numerical results are compatible with experimental ones.

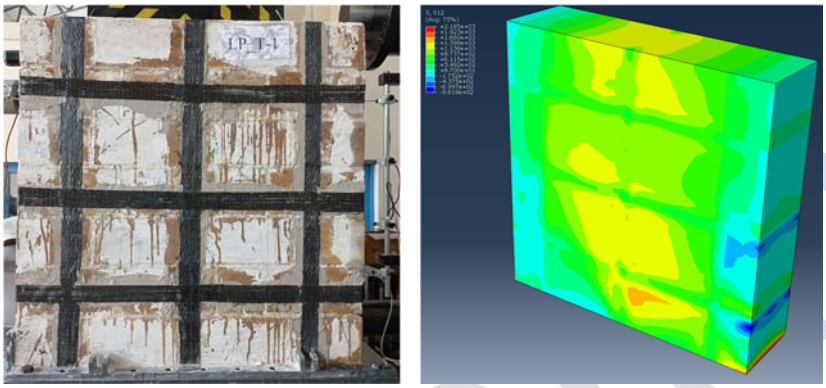

a) b)

Fig. 29 - Experimental and numerical analysis results for LP_T-S. a)Experimental crack pattern, b) Shear stress distribution

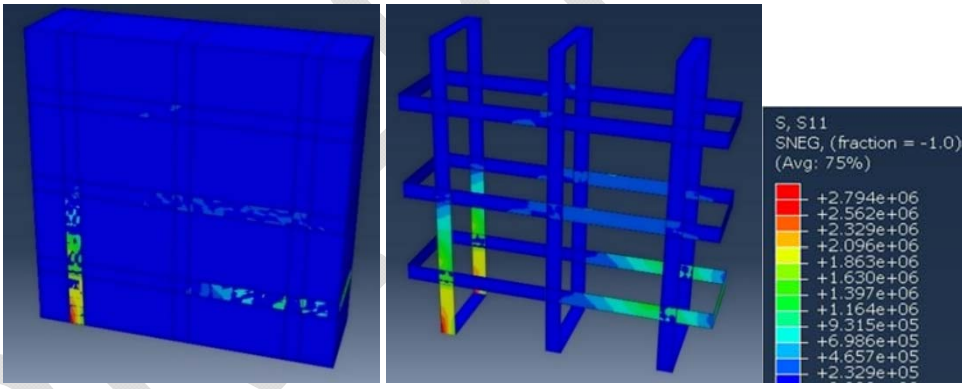

Fig. 30 - Tensile stress distribution in CFRP of LP_T-S.

4. CONCLUSIONS

This study aims to experimentally explore the structural behavior of double-wythe stone masonry walls strengthened by CFRP and grout injection under in-plane loading. Moreover, 3D NLFEA of stone masonry walls both unstrengthened and strengthening with grout injection and CFRP was performed and compared with experimental results. The following conclusions can be drawn:

1. Prior to the application of strengthening process, the masonry walls were tested under the

vertical and lateral load to induce pre-damage. After reaching the required crack width, CFRP were applied to the damaged walls, and they were subsequently retested under the same loading conditions. During the experiments, it was observed that most cracks in the unreinforced masonry stone walls propagated predominantly along the mortar joints in a staircase pattern. Notably, in the masonry units near the right toe of the walls, the increase in horizontal load led to the formation of vertical and diagonal cracks. It was observed that no new cracks occurred compared to the unstrengthened walls. However, in the toe regions of the wall, excessive crushing was observed.

2. The walls strengthened with CFRP (LP_K-S and LP_T-S) exhibited a higher displacement capacity than those reinforced with grout injection (G1-S and G2-S walls). While the ultimate displacement for G1-S and G2-S walls remained below the collapse prevention limit, LP_K-S and LP_T-S walls exceeded this threshold value. The ultimate displacement of the LP_T-S wall was slightly higher than that of the LP_K-S wall, however the lateral load-carrying capacity of LP_T-S wall was 19% higher. When the drift ratios were evaluated, it was observed that the damage levels outlined in the codes were consistent with the observed damage conditions in the walls.
3. The DP constitutive model was adopted with the macro modeling technique to simulate the nonlinear behavior of stone walls, both unstrengthened and strengthened with grout injection and CFRP. The mechanical properties obtained from the triaxial compression tests of stone, mortar, grout, and stone-mortar composite materials were used in the numerical analysis of stone masonry walls, and the results were found to be consistent. The comparisons of numerical results with the experimental ones confirm that the proposed numerical approach is appropriate for representing the lateral load-displacement relationship. Also, failure modes and peak lateral loads can reasonably be predicted using the macro modeling approach. Furthermore, it was observed that the tensile stress monitored in the CFRP grid was higher than CFRP diagonal layout.
4. The macro-modeling technique can be used quite efficiently for the analysis of masonry stone walls; however, only basic failure modes and peak lateral loads can be predicted accurately. The numerical results after the peak load (softening phase) generally differ from the experimental results. This discrepancy is believed to stem from the lack of a gradually developing damage mechanism defined in the macro modeling technique using the DP model. For future work, micro or simplified micro modeling techniques may be preferred for the numerical analysis of stone masonry walls.

Acknowledgments

This study was supported by Yildiz Technical University Research Foundation (Project No: FDK-2021-4482) and Turkish Higher Education Institution (YÖK) 100/2000 doctoral project.

Assoc. Prof. Dr. Cüneyt VATANSEVER is gratefully acknowledged for providing technical support in the use of Abaqus software.

References

[1] L. G. Baltazar, F. M. A. Henriques, and M. T. Cidade, "Experimental Study and Modeling of Rheological and Mechanical Properties of NHL Grouts," Journal of Materials in Civil Engineering, vol. 27, no. 12, pp. 1–11, Dec. 2015, doi: 10.1061/(ASCE)MT.1943-5533.0001320.

[2] B. Doran, H. Orhun Koksal, S. Aktan, S. Ulukaya, D. Oktay, and N. Yuzer, "In-Plane Shear Behavior of Traditional Masonry Walls," International Journal of Architectural Heritage, vol. 11, no. 2, pp. 278–291, Feb. 2017, doi: 10.1080/15583058.2016.1207114.

[3] P. B. Lourenço, D. V. Oliveira, P. Roca, and A. Orduña, "Dry Joint Stone Masonry Walls Subjected to In-Plane Combined Loading," Journal of Structural Engineering, vol. 131, no. 11, pp. 1665–1673, Nov. 2005, doi: 10.1061/(ASCE)0733-9445(2005)131:11(1665).

[4] P. B. Lourenço, "Computational strategies for masonry structures," Doctoral Thesis, 1996.

[5] M. Ashraf, A. N. Khan, A. Naseer, Q. Ali, and B. Alam, "Seismic Behavior of Unreinforced and Confined Brick Masonry Walls Before and After Ferrocement Overlay Retrofitting," International Journal of Architectural Heritage, vol. 6, no. 6, pp. 665–688, Nov. 2012, doi: 10.1080/15583058.2011.599916.

[6] A. Borri, G. Castori, and M. Corradi, "Shear behavior of masonry panels strengthened by high strength steel cords," Constr Build Mater, vol. 25, no. 2, pp. 494–503, Feb. 2011, doi: 10.1016/j.conbuildmat.2010.05.014.

[7] B. Doran, N. Yuzer, S. Aktan, D. Oktay, and S. Ulukaya, "Numerical Modeling of Traditional Masonry Walls Strengthened with Grout Injection," International Journal of Architectural Heritage, vol. 14, no. 10, pp. 1517–1532, Nov. 2020, doi: 10.1080/15583058.2019.1618970.

[8] Z. Multazam, K. Yamamoto, K. Timsina, C. K. Gadagamma, and K. Meguro, "Shaking table tests of a one-quarter scale model of concrete hollow block masonry houses retrofitted with fiber-reinforced paint," Sci Rep, vol. 14, no. 1, p. 8041, Apr. 2024, doi: 10.1038/s41598-024-58365-4.

[9] M. A. Elgawady and P. Lestuzzi, "A review of conventional seismic retrofitting techniques for URM," 13th International Brick and Block Masonry Conference, no. January, pp. 1–10, 2004.

[10] M. Godio, F. Vanin, S. Zhang, and K. Beyer, "Quasi-static shear-compression tests on stone masonry walls with plaster: Influence of load history and axial load ratio," Eng Struct, vol. 192, pp. 264–278, Aug. 2019, doi: 10.1016/j.engstruct.2019.04.041.

[11] M. ElGawady, M., Lestuzzi, P., Badoux, "A Review of Retrofitting of URM Walls Using Composites," in 4th International Conference on Advanced Composite Materials in Bridges and Structures, Calgary, Alberta, 2004.

[12] M. Elgawady, "Seismic in-plane behavior of URM walls upgraded with composites," 2004. doi: 10.5075/epfl-thesis-3111.

[13] T. C. Triantafillou, "Composites: a new possibility for the shear strengthening of concrete, masonry and wood," Compos Sci Technol, vol. 58, no. 8, pp. 1285–1295, Aug. 1998, doi: 10.1016/S0266-3538(98)00017-7.

[14] M. Uranjek, V. Bosiljkov, R. Žarnić, and V. Bokan-Bosiljkov, "In situ tests and seismic assessment of a stone-masonry building," Mater Struct, vol. 45, no. 6, pp. 861–879, Jun. 2012, doi: 10.1617/s11527-011-9804-z.

[15] B. Dinç-Şengönül, D. Oktay, and N. Yüzer, "Effect of temperature, resting time and brick dust (Horasan) on the rheological properties of hydraulic lime-based grouts," Constr Build Mater, vol. 265, p. 120644, 2020, doi: 10.1016/j.conbuildmat.2020.120644.

[16] B. Dinç-Şengönül, M. Bayram, D. Oktay, and N. Yüzer, "Valorization of Cappadocia waste earth in the production of sustainable lime-based grouts," Sustain Chem Pharm, vol. 38, p. 101503, Apr. 2024, doi: 10.1016/j.scp.2024.101503.

[17] L. G. Baltazar and F. M. A. Henriques, "Rheology of Grouts for Masonry Injection," Key Eng Mater, vol. 624, pp. 283–290, Sep. 2014, doi: 10.4028/www.scientific.net/KEM.624.283.

[18] L. G. Baltazar, F. M. A. Henriques, D. Rocha, and M. T. Cidade, "Experimental Characterization of Injection Grouts Incorporating Hydrophobic Silica Fume," Journal of Materials in Civil Engineering, vol. 29, no. 10, Oct. 2017, doi: 10.1061/(ASCE)MT.1943-5533.0002021.

[19] L. G. Baltazar, F. M. A. Henriques, and F. Jorne, "Optimisation of flow behaviour and stability of superplasticized fresh hydraulic lime grouts through design of experiments," Constr Build Mater, vol. 35, pp. 838–845, Oct. 2012, doi: 10.1016/j.conbuildmat.2012.04.084.

[20] L. G. Baltazar, F. M. A. Henriques, and M. T. Cidade, "Contribution To the Design Of Hydraulic Lime-Based Grouts For Masonry Consolidation," Journal of Civil Engineering and Management, vol. 21, no. 6, pp. 698–709, Jun. 2015, doi: 10.3846/13923730.2014.893918.

[21] E. Luso and P. B. Lourenço, "Experimental laboratory design of lime based grouts for masonry consolidation," International Journal of Architectural Heritage, pp. 1–10, Jul. 2017, doi: 10.1080/15583058.2017.1354095.

[22] D. V. Bompa and A. Y. Elghazouli, "Shear-Compression Failure Envelopes for Clay Brick Lime Mortar Masonry Under Wet and Dry Conditions," 2022, pp. 175–185. doi: 10.1007/978-3-030-90788-4_17.

[23] M. R. Valluzzi, F. da Porto, and C. Modena, "Behavior and modeling of strengthened three-leaf stone masonry walls," Mater Struct, vol. 37, no. 3, pp. 184–192, Apr. 2004, doi: 10.1007/BF02481618.

[24] G. Vasconcelos and P. B. Lourenço, "Experimental characterization of stone masonry in shear and compression," Constr Build Mater, vol. 23, no. 11, pp. 3337–3345, 2009, doi: 10.1016/j.conbuildmat.2009.06.045.

[25] M. Abdel-Mooty, A. Al Attar, and M. El Tahawy, "Experimental evaluation of stone masonry walls with lime based mortar under vertical loads," Structural Studies, Repairs and Maintenance of Heritage Architecture XII, vol. 118, pp. 401–412, Sep. 2011, doi: 10.2495/STR110331.

[26] D. V. Oliveira, R. A. Silva, E. Garbin, and P. B. Lourenço, "Strengthening of three-leaf stone masonry walls: an experimental research," Mater Struct, vol. 45, no. 8, pp. 1259–1276, Aug. 2012, doi: 10.1617/s11527-012-9832-3.

[27] A. Rezaie, M. Godio, and K. Beyer, "Experimental investigation of strength, stiffness and drift capacity of rubble stone masonry walls," Constr Build Mater, vol. 251, p. 118972, Aug. 2020, doi: 10.1016/j.conbuildmat.2020.118972.

[28] L. Estevan, F. J. Baeza, D. Bru, and S. Ivorra, "Stone masonry confinement with FRP and FRCM composites," Constr Build Mater, vol. 237, p. 117612, Mar. 2020, doi: 10.1016/j.conbuildmat.2019.117612.

[29] A. Sandoli, B. Ferracuti, and B. Calderoni, "FRP-confined tuff masonry columns: regular and irregular stone arrangement," Compos B Eng, vol. 162, pp. 621–630, Apr. 2019, doi: 10.1016/j.compositesb.2019.01.015.

[30] A. Rahman and T. Ueda, "Experimental Investigation and Numerical Modeling of Peak Shear Stress of Brick Masonry Mortar Joint under Compression," Journal of Materials in Civil Engineering, vol. 26, no. 9, Sep. 2014, doi: 10.1061/(ASCE)MT.1943-5533.0000958.

[31] G. Milani, T. Rotunno, E.Sacco, and A. Tralli, "Failure load of Frp strengthened masonry walls: Experimental results and numerical models," SID Structural Integrity and Durability, vol. 2, no. 1, pp. 29–50, 2006.

[32] A. Ghobarah and K. El Mandooh Galal, "Out-of-Plane Strengthening of Unreinforced Masonry Walls with Openings," Journal of Composites for Construction, vol. 8, no. 4, pp. 298–305, 2004, doi: 10.1061/(asce)1090-0268(2004)8:4(298).

[33] B. Bozyigit et al., "Damage to monumental masonry buildings in Hatay and Osmaniye following the 2023 Turkey earthquake sequence: The role of wall geometry, construction quality, and material properties," Earthquake Spectra, vol. 40, no. 3, pp. 1870–1904, Aug. 2024, doi: 10.1177/87552930241247031.

[34] A. Bayraktar, N. Coşkun, and A. Yalçin, "Performance of Masonry Stone Buildings during the March 25 and 28, 2004 Aşkale (Erzurum) Earthquakes in Turkey," Journal of Performance of Constructed Facilities, vol. 21, no. 6, pp. 432–440, Dec. 2007, doi: 10.1061/(ASCE)0887-3828(2007)21:6(432).

[35] C. Demir and A. Ilki, "Characterization of the materials used in the multi-leaf masonry walls of monumental structures in Istanbul, Turkey," Constr Build Mater, vol. 64, pp. 398–413, Aug. 2014, doi: 10.1016/j.conbuildmat.2014.04.099.

[36] A. Bayraktar, N. CoŞkun, and A. Yalçin, "Damages of masonry buildings during the July 2, 2004 Doğubayazıt (Ağrı) earthquake in Turkey," Eng Fail Anal, vol. 14, no. 1, pp. 147–157, Jan. 2007, doi: 10.1016/j.engfailanal.2005.11.011.

[37] B. Dinç-Şengönül, N. Yüzer, C. Şengönül, S. Ulukaya, D. Oktay, and Ö. Ündül, "Behavior of grout injected solid stone masonry walls under in-plane loading," Structures, vol. 58, p. 105411, Dec. 2023, doi: 10.1016/j.istruc.2023.105411.

[38] General Directorate of Highways B.D.H.B.B., Historical Bridges, No: 268. Ankara, 2009.

[39] N. Mazzon, "Infuence of Grout Injection on the Dynamic Behaviour of Stone Masonry Buildings," 2010.

[40] M. Ponte, J. Milosevic, and R. Bento, "Parametrical study of rubble stone masonry panels through numerical modelling of the in-plane behaviour," Bulletin of Earthquake Engineering, vol. 17, no. 3, pp. 1553–1574, Mar. 2019, doi: 10.1007/s10518-018-0511-9.

[41] B. Silva, M. Dalla Benetta, F. da Porto, and C. Modena, "Experimental assessment of in-plane behaviour of three-leaf stone masonry walls," Constr Build Mater, vol. 53, pp. 149–161, Feb. 2014, doi: 10.1016/j.conbuildmat.2013.11.084.

[42] G. Vasconcelos and P. B. Lourenço, "In-Plane Experimental Behavior of Stone Masonry Walls under Cyclic Loading," Journal of Structural Engineering, vol. 135, no. 10, pp. 1269–1277, Oct. 2009, doi: 10.1061/(ASCE)ST.1943-541X.0000053.

[43] EN 1015-11, Methods of test for mortar for masonry - Determination of flexural and compressive strength of hardened mortar. 2019.

[44] EN 13286-43, Unbound and hydraulically bound mixtures - Part 43: Test method for the determination of the modulus of elasticity of hydraulically bound mixtures. 2017.

[45] E. Y. Gökyiğit-Arpaci, D. Oktay, N. Yüzer, S. Ulukaya, and D. Ekşi-Akbulut, "Performance Evaluation of Lime-Based Grout Used for Consolidation of Brick Masonry Walls," Journal of Materials in Civil Engineering, vol. 31, no. 6, Jun. 2019, doi: 10.1061/(ASCE)MT.1943-5533.0002692.

[46] TS EN 1926, Natural stone test methods- Determination of compressive strength. 2007.

[47] TS EN 12372, Natural stone test methods- Determination of flexural strength under concentrated load. 2007.

[48] BS EN 1771, Products and systems for the protection and repair of concrete structures. Test methods. Determination of injectability and splitting test. British Standards. 3. 2004.

[49] B. Biçer-şimşir, I. Griffin, B. Palazzo-Bertholon, and L. Rainer, "Lime-based injection grouts for the conservation of architectural surfaces," Studies in Conservation, vol. 54, no. sup1, pp. 3–17, Jun. 2009, doi: 10.1179/sic.2009.54.Supplement-1.3.

[50] V. Pachta, "The Role of Glass Additives in the Properties of Lime-Based Grouts," Heritage, vol. 4, no. 2, pp. 906–916, May 2021, doi: 10.3390/heritage4020049.

[51] V. Pachta, F. Papadopoulos, and M. Stefanidou, "Development and testing of grouts based on perlite by-products and lime," Constr Build Mater, vol. 207, pp. 338–344, May 2019, doi: 10.1016/j.conbuildmat.2019.02.157.

[52] V. Pachta and D. Goulas, "Fresh and hardened state properties of fiber reinforced lime-based grouts," Constr Build Mater, vol. 261, p. 119818, Nov. 2020, doi: 10.1016/j.conbuildmat.2020.119818.

[53] M. Stefanidou, V. Pachta, and G. Konstantinidis, "Exploitation of waste perlite products in lime-based mortars and grouts," Sustain Chem Pharm, vol. 32, p. 101024, May 2023, doi: 10.1016/j.scp.2023.101024.

[54] S. Aktan, "Düzlem İçi Yükler Etkisindeki Yığma Duvarlarda Bünyesel Modelleme," Doktora tezi, Yıldız Teknik Üniversitesi, İstanbul, 2016.

[55] D. V Oliveira and P. B. Lourenço, "Experimental behaviour of three-leaf stone masonry walls," 2006.

[56] M. Corradi, C. Tedeschi, L. Binda, and A. Borri, "Experimental evaluation of shear and compression strength of masonry wall before and after reinforcement: Deep repointing," Constr Build Mater, vol. 22, no. 4, pp. 463–472, Apr. 2008, doi: 10.1016/j.conbuildmat.2006.11.021.

[57] K. F. Abdulla, L. S. Cunningham, and M. Gillie, "Simulating masonry wall behaviour using a simplified micro-model approach," Eng Struct, vol. 151, pp. 349–365, Nov. 2017, doi: 10.1016/j.engstruct.2017.08.021.

[58] H. O. Koksal, O. Jafarov, B. Doran, S. Aktan, and C. Karakoc, "Computational material modeling of masonry walls strengthened with fiber reinforced polymers," Structural Engineering and Mechanics, vol. 48, no. 5, pp. 737–755, Dec. 2013, doi: 10.12989/sem.2013.48.5.737.

[59] B. Doran, S. Ulukaya, Z. Unsal Aslan, M. Karslioglu, and N. Yuzer, "Experimental Investigation of CFRP Strengthened Unreinforced Masonry Walls with Openings," International Journal of Architectural Heritage, vol. 16, no. 12, pp. 1907–1920, Dec. 2022, doi: 10.1080/15583058.2021.1918286.

[60] B. Doran, M. Karslioglu, Z. Unsal Aslan, and C. Vatansever, "Experimental and Numerical Investigation of Unreinforced Masonry Walls with and without Opening," International Journal of Architectural Heritage, vol. 17, no. 11, pp. 1833–1854, Nov. 2023, doi: 10.1080/15583058.2022.2080611.

[61] B. Dinç-Şengönül, Y. Hothot, B. Doran, N. Yüzer, S. Ulukaya, and D. Oktay, "Nonlinear Behaviour of Two-Whyte Stone Walls," in 12th International Conference on Structural Analysis of Historical Constructions SAHC 2020, Barcelona, 2021, pp. 1–10. doi: 10.23967/sahc.2021.167.

[62] "ABAQUS 6.14/CAE Analysis User's Manual," Dassault Systems, Simulia Corporation: 6.14.

[63] İ. E. Bal, "Yığma yapılarda doğrusal olmayan artımsal analiz için bir yöntem önerisi," Dicle Üniversitesi Mühendislik Fakültesi Mühendislik Dergisi, vol. 8, no. 3, pp. 463–474, 2017, [Online]. Available: https://dergipark.org.tr/tr/pub/dumf/issue/33629/405219

[64] J. Scacco, B. Ghiassi, G. Milani, and P. B. Lourenço, "A Fast Modeling Approach for Numerical Analysis of Unreinforced and FRCM Reinforced Masonry Walls Under Out-Of-Plane Loading," Composites Part B, p. 107553, 2019, doi: 10.1016/j.compositesb.2019.107553.

[65] Y. M. Hothot, B. Dinç-Şengönül, B. Doran, and N. Yüzer, "Nonlinear Finite Element Analysis of Stone Masonry-Solid Wall," in 6 th International Conference on Earthquake Engineering and Seismology, Gebze, Kocaeli, 2021.

[66] Y. M. Hothot, B. D. Şengönül, B. Doran, and N. Yüzer, "Finite Element Applications of Stone Masonry Walls," in 14th International Congress on Advances in Civil Engineering (ACE2020-21), İstanbul, 2021, pp. 1–6.

[67] W. F. Chen, Plasticity in Reinforced Concrete. J. Ross Publishing, 2007.

[68] H. B. Kaushik, D. C. Rai, and S. K. Jain, "Stress-strain characteristics of clay brick masonry under uniaxial compression," Journal of Materials in Civil Engineering, vol. 19, no. 9, pp. 728–739, 2007, doi: 10.1061/(ASCE)0899-1561(2007)19:9(728).

[69] H. O. KÖKSAL and H. YILDIRIM, "Eksenel basınç altında beton briket yığma prizmaların sonlu eleman analizi," Teknik Dergi, vol. 15, no. 3, pp. 3249–3265, 2004, [Online]. Available: https://search.trdizin.gov.tr/tr/yayin/detay/1104

[70] T. Paulay and M. J. N. Priestly, Seismic Design of Reinforced Concrete and Masonry Buildings. 1992.

[71] A. Brencich, C. Corradi, and L. Gambarotta, "Compressive strength of solid clay brick masonry under eccentric loading," Proceedings British Masonry Society, pp. 37–46, 2002.

[72] G. , Mohamad, P. B. , Lourenço, and H. R. Roman, "Mechanical behavior assessment of concrete block masonry prisms under compression.," 2005.

[73] O. , Jafarov, "Lifli Polimerle Güçlendirilmiş Yığma Duvarların Modellenmesi, Doktora Tezi, Yıldız Teknik Üniversitesi Fen Bilimleri Enstitüsü, İstanbul.," 2012.